CHEMISTRY OF MATERIALS

pubs.acs.org/cm

Article

Adhesive Properties of Semiconducting Polymers: Poly(3-alkylthiophene) as an Ersatz Glue

Alexander X. Chen, Silpa S. Pazhankave, Jordan A. Bunch, Allison Lim, Kartik Choudhary, Guillermo L. Esparza, Rory Runser, Christian G. Hoover, and Darren J. Lipomi*

Cite This: *Chem. Mater.* 2023, 35, 3329−3342

Read Online

ACCESS | Metrics & More | Article Recommendations | Supporting Information

ABSTRACT: The functionality and usability of π-conjugated (semiconducting) polymers is dependent on the adhesive and interfacial properties of the solid film. Such properties are critical in devices incorporating semiconducting polymers because these layers serve both an active and structural role. They are load bearing in the sense that bending, stretching, scratching, and impact places stress within the semiconducting film at the interfaces with other layers in the device stack. Thus, these organic semiconductors must have good cohesive and adhesive properties despite being designed primarily for optoelectronic function (as opposed to mechanical stability). Here, we measure the effect of the alkyl side chain length on the mechanical and adhesive properties of poly(3-alkylthiophene) (P3AT) using three different measurement techniques not often applied to conjugated polymers: nanoindentation (quasi-static and dynamic), a lap-joint shear test, and adhesive peel tests (90 and 180°). We performed these measurements alongside pseudo-free-standing ("film-on-water") tensile tests commonly reported in the literature. We find a monotonic relationship between the length of the side chain and parameters associated with the storage of energy: decreased elastic modulus, strength, and resilience and increased elastic range, from the shortest to the longest side chain. However, we observed a maximum in toughness, fracture strain, and adhesive energy dissipation at A = heptyl or octyl, as well as differences in debonding behavior when P3AT films were deposited on top of a poly(3,4-ethylenedioxythiophene):poly(styrene sulfonate) (PEDOT:PSS) film. Notably, our findings suggest that an increase in the alkyl side chain length (beyond n = 8 for P3ATs) may be detrimental to adhesion and thus mechanical robustness.

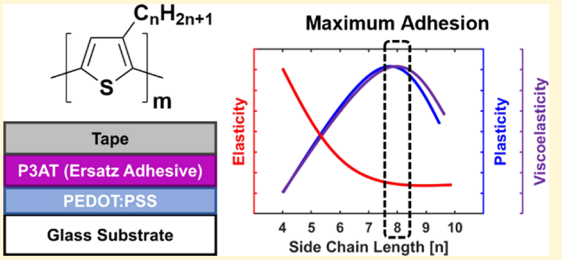

INTRODUCTION

The promise of π-conjugated (semiconducting) polymers is to combine the electronic functionality of conventional semiconductors with the processability and deformability of plastics. Conjugated polymers are widely investigated as active components in organic bioelectronic and optoelectronic devices.[1−9] These materials are especially attractive for applications that must withstand the rigors of wearability and the outdoor environment. Thus, their usability and functionality depend on the ability of the polymer to store or dissipate mechanical energy without failure of the device.[10] For this reason, a significant body of literature is dedicated to understanding the mechanical properties of conventional polymers and engineering plastics.[11] Work by Seitz has shown that mechanical properties of a solid polymer film can often be predicted from five molecular properties: the molecular weight,[12] van der Waals volume, length and number of rotational bonds in the monomer structure, and glass transition temperature.[13] However, for semiconducting polymers, which are composed of π-conjugated backbones that discourage deformation—along with pendant groups that encourage it—such simple models have failed to predict the subtleties of the thermomechanical behavior, particularly as the length of the pendant group increases. Moreover, thermomechanical stability must be balanced with electronic performance.

Several recent strategies, including crosslinking of the side chains,[14−18] aggregation of polymer molecules into coiled nanofibers,[19−21] and copolymerization,[22−31] have succeeded in many ways to combine electronic function and mechanical deformability. Despite this success, there remain important questions as to what structural parameters should be engineered to obtain specific mechanical outcomes. Of course, the polymer must have sufficient cohesive energy to retain favorable charge-transport properties when bent or deformed. However, conjugated polymer films must also have strong mechanical interfaces with other layers in multilayer devices. The semiconducting film thus acts as an "ersatz glue"; it must

Received: March 2, 2023
Revised: March 24, 2023
Published: April 4, 2023

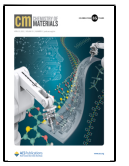

function as an adhesive within a device, despite not being designed to do so.

The way in which mechanical energy is absorbed and dissipated within a semiconducting polymer film is governed by its molecular structure and the way that structure assembles itself in the solid state.[32] For a device stack comprising multiple polymeric films that are deposited sequentially, the interactions between the layers—including physical interpenetration and electrostatic effects—also influence the adhesive strength at the interface.[32,33] As in a purpose-designed adhesive (e.g., sticky tape), mechanical work can also be dissipated by the viscoelastic behavior of the semiconducting polymer. Adhesive properties[34] are thus determined by both the properties of the bulk and of the interfaces.[32,35,36] For semiconducting polymers, adhesive properties having their origins in electrostatics[37] (e.g., van der Waals forces) are influenced by the presence of polar and polarizable groups, the ratio of saturated to unsaturated bonds, the packing density of the film, and possibly the molecular orientation (texture) at the surface.[33] Adhesive properties arising from molecular dynamics—including interpenetration and viscoelasticity—are influenced by molecular weight and dispersity, as well as the inclusion of tackifiers, plasticizers, and dopants.[38−40] The mechanical properties are also influenced extrinsically by processing methods, operating temperature, and thermal history.[32,35,38]

The type of fracture obtained depends on the details of energy dissipation at the crack tip, which depends both on molecular structure and extensive parameters (e.g., thickness). For example, Dauskardt and co-workers measured greater energies of decohesion as the thickness of the poly(3-hexylthiophene):[6,6]-phenyl-C_{61}-butyric acid methyl ester (P3HT:PCBM) film increased (for P3HT with molecular weights of 53−100 kDa). The reason for this increase in measured decohesion energy was attributed to the larger plastic zone at the crack tip in thicker films, which allows for the dissipation of mechanical work, thus impeding the growth of the crack.[41] However, for P3HT with a molecular weight of 28 kDa, the authors found that the decohesion energy was not affected by the film thickness due to the decreased plasticity (and viscoelasticity) of the film at the crack tip.[41,42] The mechanisms associated with the de-adhesion of viscoelastic materials are also dependent on, e.g., the angle of the peel, the rigidity of the substrate, and the rigidity of the adherend.[43−45] Previous work from our laboratory has shown that in roll-to-roll printed devices, encapsulation allows P3HT:PCBM solar cells to withstand thousands of cycles of torsion and bending.[46] However, mechanical delamination eventually occurs due to crazing near the rough perimeter edges of the barrier layer, which propagates under continued deformation and results in adhesive failure at the interface between the PEDOT:PSS and the active layer as well as decohesion within the active layer.

The alkyl pendant groups attached to the main chain of conjugated polymers are significant determinants of the thermomechanical properties of the solid polymer film. Rigid π-conjugated backbones have limited conformational flexibility, and thus the entropic driving force for solubility is limited. The presence of alkyl chains affords greater conformational freedom and thus increased solubility.[47] In the solid state, the side chains increase the free volume and decrease the van der Waals energy between the π-conjugated main chains. These effects combine to reduce the activation energy required to translate the chains past one another. Likewise, the greater free volume also contributes to greater conformational mobility (e.g., twisting, bending) along the backbone.[48] Thus, an increase in alkyl chain length leads to a decrease in the glass transition temperature (T_g)[49,50]—i.e., the α-transition temperature—of the backbone and thus elastic modulus.[51,52] In contrast, the thermal transition associated with relaxation of the pendant group (i.e., β-transition) increases with increasing side chain length.[49,53,54] At an operating temperature above T_g, secondary thermal relaxation mechanisms are dependent on both the α-transition and β-transition temperatures, and allow for dissipation of kinetic energy in both the disordered (amorphous) and ordered phases (e.g., relaxation of aggregates, chain slip in crystallites).[48,55] Additional transitions are likely to be present in polymers with structures more complex than P3ATs, e.g., donor−acceptor polymers, which have two or more monomer subunits and may have branched side chains.[56]

Here, we used the well-known class of semiconducting polymer, regioregular poly(3-alkythiophene) (P3AT), as a model polymer. A number of studies have elucidated the effect on the linear side chain length on the mechanical properties in P3ATs.[57] For example, our laboratory has investigated the effects of side chain length and molecular weight on the scratch resistance and tensile behavior of P3AT thin films.[58−60] Progressive-load scratch testing determined that an increase in the alkyl chain length led to a decrease in both cohesion and adhesion on silicon substrates.[58] Likewise, our group and others have used the buckling methodology[61] and quasi-free-standing tensile testing methodology (film-on-water)[62,63] to measure the elastic modulus relative to increasing length of the alkyl chain; the modulus was found to decrease monotonically. With regard to optoelectronic properties, studies have shown that a longer side chains in P3ATs typically corresponds to a decreased conductivity,[64] increased luminescence,[64−66] decreased hole mobility (as measured using organic field-effect transistors,[67−69] although the effect is not always monotonic[70,71]), and increased barriers to hole injection.[72] In solar cells, the side chain length of P3ATs have been shown to be a significant determinant of the photovoltaic properties of P3AT:fullerene[51,73−75] (and P3AT:non-fullerene[76−78]) heterojunctions, all-polymer heterojunctions,[79,80] and perovskite solar cells.[81]

A comparatively smaller body of literature has studied the adhesive properties of P3ATs (or other conjugated polymers). A notable exception has been the work of Dauskardt and co-workers, who have made extensive use of the four-point-bend and double-cantilever beam tests to understand how the morphology and composition of layers within an organic solar cell control adhesive and cohesive debonding behavior.[41,82−90] For example, Bruner and Dauskardt found that the cohesion energy[41] and resistance to decohesion growth[82] of a P3HT:PCBM bulk heterojunction increased from ∼2 to ∼17 J m^{-2} as the molecular weight of P3HT increased. Choi et al. later extended this work to an acceptor-type polymer, which also exhibited increased fracture energy with increasing molecular weight.[88] Dupont et al. found that the presence of moisture drove the cohesive debonding of PEDOT:PSS films, which are commonly used as hole transporting layers in organic solar cells.[89] Brand et al. determined that debonding in a P3HT:PCBM solar cell always occurred cohesively within the bulk heterojunction, with an increasing mass ratio of P3HT (up to 75%) corresponding to an increase in fracture energy.[42] This fracture mechanism within the P3HT:PCBM bulk heterojunction has been attributed to tensile strain resulting

https://doi.org/10.1021/acs.chemmater.3c00485
Chem. Mater. 2023, 35, 3329−3342

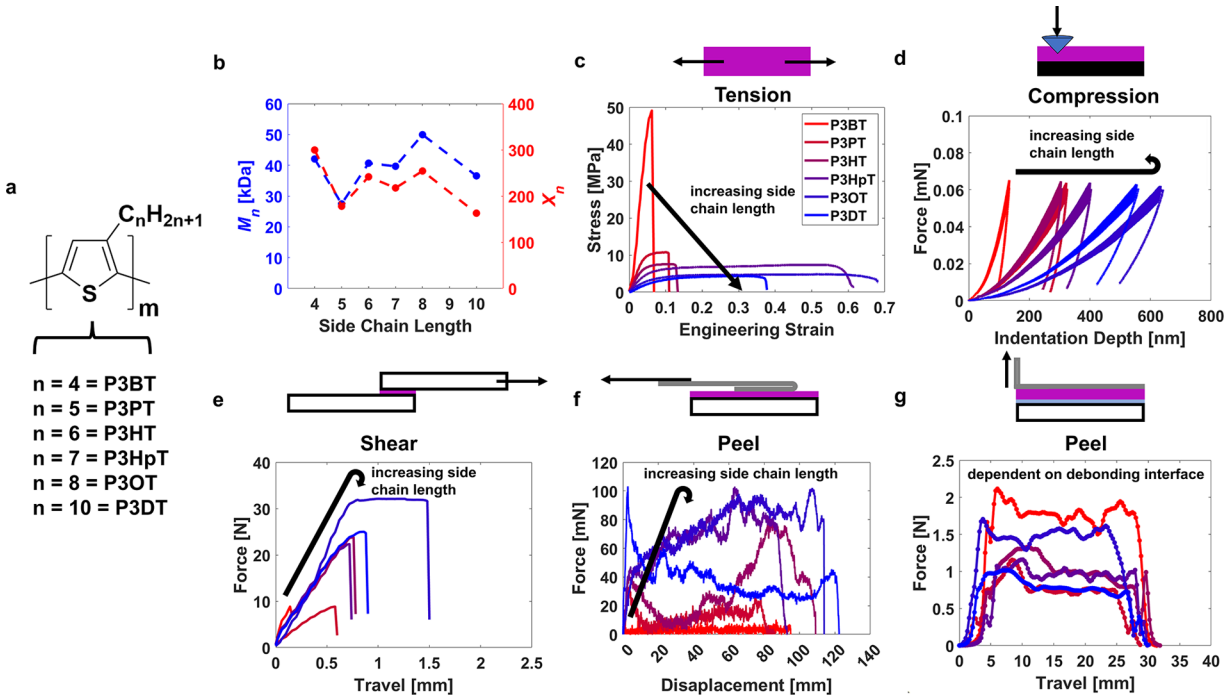

Figure 1. (a) Chemical structure of the poly(3-alkylthiophene) (P3AT) library investigated in this study. (b) Number-averaged molecular weight (M_n) and degree of polymerization (X_n) for each polymer in the library. (c–g) Summary of the (c) tensile, (d) compressive (oscillatory), (e) lap-joint shear, (f) 180° peel (glass/P3AT/tape), and (g) 90° peel (glass/PEDOT:PSS/P3AT/tape) measurements performed in this study. Representative data are shown in each plot. The black arrows in (c–f) are to guide the eye to the trends in the data.

in the delamination of P3HT chains from the fullerene interface, resulting in crazing.[91] Bruner et al. has shown that molecular intercalation of fullerene acceptors in organic bulk heterojunctions increases the cohesion energy, but increasing mass ratio of the fullerene decreases the cohesion energy.[92] Other work has studied the effect of processing conditions (e.g., deposition processes,[83,93] humidity,[94] thermal annealing,[94−96] UV irradiation[94]) on the adhesive and cohesive properties. For example, Dupont et al. have found that thermal annealing can be used to modulate the interdiffusion at the P3HT:PCBM and PEDOT:PSS interface and increase the fracture energy.[94−96]

In this study, we probe the effect of the length of the alkyl side chain[57] (n = butyl, pentyl, hexyl, heptyl, octyl, and decyl) on the tensile, compressive, viscoelastic, and adhesive properties of P3AT films. Here, we use the film-on-water test, combined with three other tests conventionally used for coatings and adhesives but not generally applied to conjugated polymers: compressive nanoindentation (quasi-static and oscillatory), lap-joint (shear) tests, and peel tests. We use peel tests (rather than, e.g., double-cantilever beam tests) to evaluate the effect of a flexible adherend on the debonding behavior of the film, as conjugated polymers are likely to be used in flexible and stretchable form factors, as opposed to rigid ones.

EXPERIMENTAL DESIGN

Material Selection and Mechanical Testing. Poly(3-alkylthiophene)s were used as model polymers because they are widely studied in the literature and readily available from commercial vendors. In order to reduce the effect of entanglement density on the measured properties, we used P3ATs with comparable molecular weights as reported by the vendors (and remeasured by us using gel permeation chromatography[97]), degrees of polymerization, and regioregularity (Table S3). Likewise, the molecular weight of all P3ATs were selected to be above the entanglement molecular weight of P3HT (typically ∼10 to 20 kDa).[10,98] Detailed descriptions about the materials used are contained in the Supporting Information. We chose several modes of mechanical measurement because envisioned applications of semiconducting polymers are likely to be subjected to tensile, compressive, shearing, and peeling forces. Thus, we measured the mechanical properties five ways: a pseudo-free-standing tensile test (tensile properties), nanoindentation (compressive properties),[99−103] lap-joint shear tests (shear properties), 180° peel tests for a glass/P3AT interface (adhesive peel force), and 90° peel tests for a PEDOT:PSS/P3AT interface (peel force, debonding behavior). We choose to use peel tests to evaluate the debonding behavior from a flexible adherend (e.g., adhesive tape) rather than a rigid adherend (e.g., a glass substrate).

Tensile tests and 90° peel tests were conducted with spin coated films. However, because nanoindentation required thicker films (as to reduce the impact of the silicon substrate on the measurement), drop casting was used to form the films (yielding films with thicknesses of ∼4 μm). For adhesion measurements (i.e., lap-joint shear tests and 180° peel tests), blade coating was used to deposit films on top of rectangular glass substrates, for which the measured adhesion is dependent on both layers (e.g., both the polymer film and the substrate). Here, we selected glass as the substrate in order to ensure a sharp interface with weak molecular force (i.e., with no covalent bonds or chemical interactions).[32] The goal of this selection was to evaluate the functionality of these films as viscoelastic adhesives (in which the dissipation of energy is mediated by chain reptation, entropy, intermolecular forces, and the stretching and breakage of covalent bonds). However, in device applications, the conjugated polymer film is likely to interface with another thin, flexible layer. Semiconducting polymers are incorporated in a variety of devices, and thus a broad range of interfaces must be considered. (Trends in adhesive and debonding behavior are unlikely to be universal, as adhesion is dependent on both surfaces in contact.) In this study, we conducted 90° peel tests where P3AT films are deposited on top of a PEDOT:PSS layer, which is ubiquitously used as a hole transport layer in organic solar cells.

https://doi.org/10.1021/acs.chemmater.3c00485
Chem. Mater. 2023, 35, 3329−3342

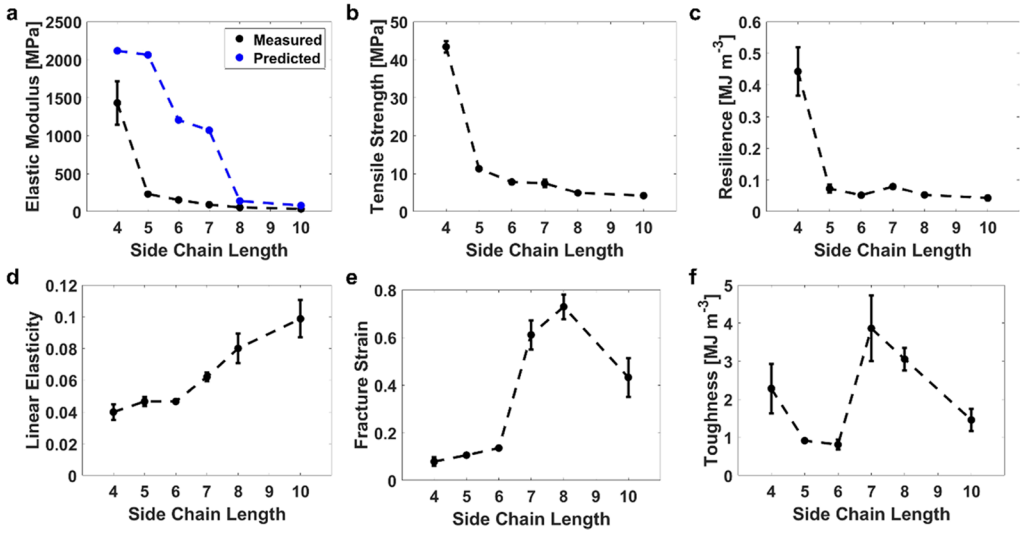

Figure 2. (a) Elastic modulus (measured and predicted), (b) tensile strength, (c) resilience, (d) linear elasticity, (e) fracture strain, and (f) toughness relative to side chain length as extracted from tensile measurements.

Theoretical Calculations. Semi-empirical relationships between the mechanical properties and molecular characteristics of conventional (non-conjugated) polymers were developed by Seitz.[13] Here, we used methods developed by Seitz[13] and Fedors[104] (and later applied to conjugated polymers by Tahk et al.[105] and Savagatrup et al.[106]) to calculate the theoretical tensile modulus (E), bulk modulus (B), and cohesive energy (E_{coh}). Measured values for T_g of each P3AT were extracted from literature[49,107−109] and used in these calculations. These calculated values were used as a guide and comparison for our measurements. Detailed methodologies are included in the Supporting Information (Figure S1, Tables S1 and S2).

Characterization of P3AT Films. Characterization of the morphological and molecular characteristics of each P3AT film were performed to elucidate how such characteristics govern the bulk and interfacial properties of P3ATs. Gel permeation chromatography (GPC) was used to measure the molecular weight and dispersity of each P3AT (Table S3), while ultraviolet−visible (UV−vis) spectroscopy was used to determine the aggregation. The surface energy was calculated from contact angle measurements with water and diiodomethane using the harmonic mean Wu model.[110] Finally, atomic force spectroscopy (AFM) was used to elucidate changes in film topography relative to side chain length.

RESULTS AND DISCUSSION

We summarize the mechanical characterization conducted in this work on a series of poly(3-alkylthiophene)s (P3ATs) in Figure 1. The mechanical properties were compared using two modes of deformation: tension and compression. Likewise, the adhesive behavior was evaluated using three measurements: lap-joint shear tests, 180° peel tests (glass/P3AT/tape), and 90° peel tests (glass/PEDOT:PSS/P3AT/tape). We elected to use P3ATs with comparable number-average molecular weights (with the caveat that Koch et al. has shown that gel permeation chromatography, when calibrated with polystyrene standards, overestimates the molecular weight of P3HT by a factor of 1.67[111]) and degrees of polymerization (X_n) in order to isolate the effect of chemical structure on the mechanical properties (Figure 1b, Table S3).

The tensile properties, as extracted from the stress−strain curves (Figure 1c), are shown in Figure 2. An increase in the side chain length makes it more favorable (i.e., requiring less mechanical energy) for a polythiophene chain to stretch and deform, which corresponds to a monotonic decrease in the elastic modulus (Figure 2a, Table S4), tensile strength (Figure 2b), and resilience (Figure 2c) of the solid film, along with a monotonic increase in linear elasticity (Figure 2d). We find the chemical structure to be a dominant determinant in the storage of energy (i.e., entropic elasticity for low-T_g P3ATs, molecular stiffness and Lennard-Jones interactions for high-T_g P3ATs) from which emerge monotonic relationships between the elastic parameters and the side chain length (Figure 2a−d).

We find that the measured tensile modulus was lower than predicted for all P3ATs (Figure 2a, Tables S2 and S4). The predicted model agrees best for P3ATs with the shortest (P3BT) and longest (P3OT, P3DT) alkyl chains, with calculations suggesting moduli about twice that of measured values. However, the moduli for P3PT, P3HT, and P3HpT differed significantly between experiment and theory, by about one order of magnitude (Table S2). These observed differences suggest that empirical correlations determined from the mechanical behavior of conventional polymers do not apply perfectly to conjugated materials, particularly for those with glass transitions near the operating temperature (∼37 to −12 °C for P3PT to P3HpT) and thus likely demonstrate both glassy and rubbery behavior (Figure S2). One reason for this misalignment could be the significantly greater difference between the thermal transitions associated with the backbone and the side chain for conjugated polymers as opposed to polymers with non-conjugated backbones.

When deformation extends beyond the elastic regime, dissipation of energy is manifested as plastic deformation, cracking, or fracture of the polymer film. Here, dissipation occurs by the disruption of intermolecular interactions (e.g., $\pi-\pi$ stacking), active slip (e.g., along the (100) and (010) planes),[112] chain pullout, and by the breaking of covalent bonds. Previous studies have shown that increasing the length of the alkyl side chain can allow for greater ordering, as well as the formation of interdigitated (e.g., "Form II") structures, which can in some circumstances lead to brittle behavior.[113,114] However, the usual result of an increase in the alkyl chain length is to increase the lamellar spacing[115] and to decrease the $\pi-\pi$ stacking.[67,69,116] These effects suggest a weakening of van der Waals forces between polymer chains.

https://doi.org/10.1021/acs.chemmater.3c00485
Chem. Mater. 2023, 35, 3329−3342

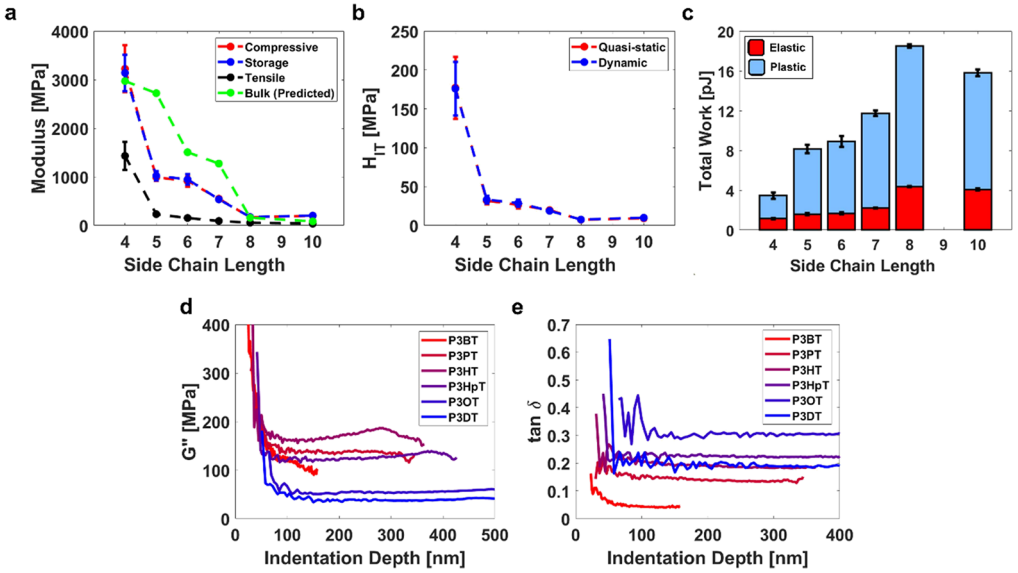

Figure 3. (a) Elastic modulus (measured and predicted) and (b) indentation hardness were extracted from quasi-static nanoindentation measurements, while (c) work, (d) loss modulus, and (e) tan δ were extracted from dynamic (oscillatory) measurements. The tensile modulus is included in the comparison of moduli for reference.

Whereas the parameters associated with elasticity exhibited monotonic relationships with the length of the alkyl side chain (Figure 2a–d), those associated with plasticity—namely fracture strain and toughness (Figure 2e,f), exhibited maxima. First, there was a significant increase in fracture strain from P3HT (n = 6) to P3HpT (n = 7), likely due to T_g of P3HpT being significantly lower than room temperature. Second, there appeared to be diminishing returns to increasing the fracture strain as the side chain length increases. An increase in side chain length from P3HpT (n = 7) to P3OT (n = 8) resulted in a similar fracture strain, while that of P3DT (n = 10) was lower. It is possible the decrease in fracture strain is in part due to a comparatively low degree of polymerization for P3DT relative to P3OT (Table S3). However, AFM experiments by Jiang et al. investigating the unfolding behavior of P3AT chains show that a single P3OT chain can extend further than a single P3DT chain (ΔL of ∼14 nm compared to ∼12 nm).[117] Likewise, buckling experiments by Printz et al. suggest that both the fracture strain and yield point of P3OT are greater than that of P3DDT (n = 12).[60] Thus, previous literature suggests that the decrease in fracture strain from n = 8 to n = 10 cannot solely be explained here by differences in degree of polymerization. Rather, the maximum in fracture strain (which occurs around n = 7–8) may represent a compromise between competing effects. That is, as the side chain is lengthened, the glass transition temperature decreases and the film becomes more ductile. However, if the increase in the length of the alkyl chain is too much, the volume fraction of load-bearing covalent bonds in the main chain is diluted to the point where the solid becomes waxy and loses its cohesion.

The toughness, taken as the energy density absorbed by a solid prior to fracture, exhibits a similar maximum around n = 7–8 (Figure 2f) owing to the large extensibility of these two entries in the series. Interestingly, the toughness of P3BT (n = 4) is nearly as high. We attribute this behavior to the extraordinarily large tensile strength exhibited by the glassiest (T_g ∼ 65 °C[107]) of P3ATs tested (Figure 1c, red curve). At an operating temperature significantly below the glass transition, the brittleness (and high strength) stems from the glassy nature of the polymer. Nevertheless, we observed some plastic flow beyond the regime of linear elasticity for P3BT (Figure S3), suggesting some mobility despite the kinetically frozen structure.[48]

The compressive properties, as extracted from nanoindentation measurements (Figure 1d), are shown in Figure 3. Again, we found essentially monotonic relationships between the elastic properties (elastic modulus, hardness, elastic work) and the alkyl chain length (Figure 3a–c), for both quasi-static and dynamic (oscillatory) measurements. However, we do observe a greater modulus (and decreased elastic work) for P3DT in comparison to P3OT. Previous studies have observed greater crystalline fractions in n = 10, 12 compared to n = 8,[54] which likely result in this increased modulus. It is also possible that the slow drying kinetics (due to the solidification process of a drop-cast film) and long alkyl side chain allow for the formation of morphological structures (e.g., nanowhiskers and nanoribbons resulting in greater π–π stacking[118]) that contribute to this difference in mechanical behavior. Under compression, the measured moduli were significantly greater than those extracted from tensile measurements (Figure 3a, Table S4). We attribute this difference to the decrease in film volume under compression in comparison to an increase under tension (i.e., the elastic modulus is related to the compressive modulus by Poisson's ratio[13]). Under real (i.e., non-theoretical) measurements, larger differences between the compressive and tensile moduli can be observed due to the behavior of defects within the solid film under the two modes of measurement.[59] For example, under tension, void spaces are stretched, propagating fracture as the size of the defect grows (i.e., crazing). Under compression, while localized deformation still occurs, some cracks and fracture interfaces can be closed, slowing down compaction and preventing fracture from propagating across larger length scales.[119] Previous work has shown similar increases in measured elastic modulus (and tensile strength) for films of poly(methyl methacrylate) between measurements under tension and compression.[120]

https://doi.org/10.1021/acs.chemmater.3c00485
Chem. Mater. 2023, 35, 3329–3342

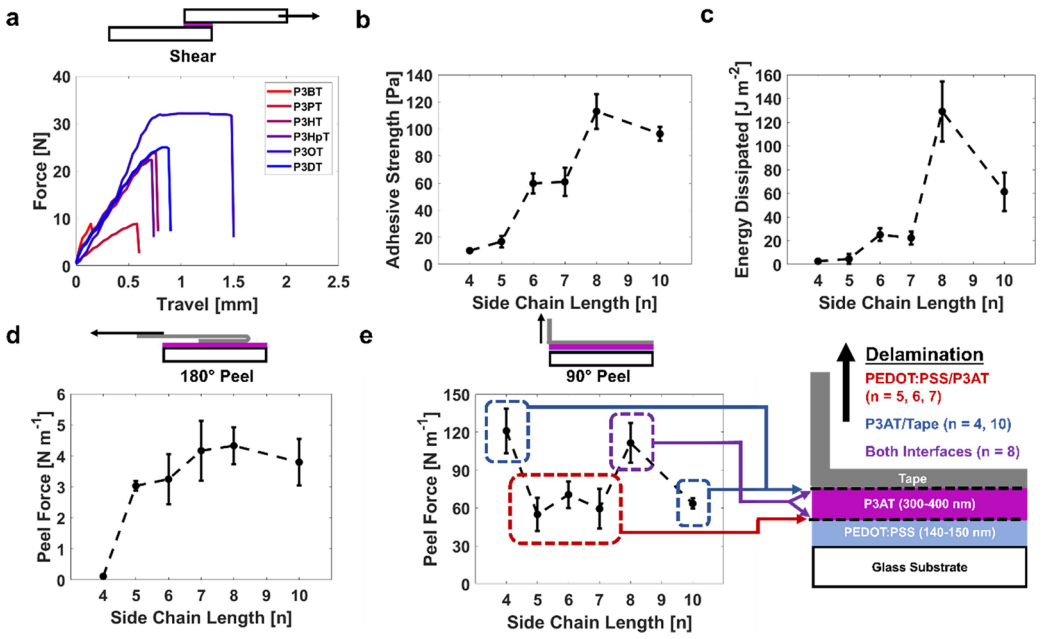

Figure 4. (a) Lap-joint shear tests were conducted on glass substrates glued together by each P3AT film (for which representative force−displacement curves are shown) from which the (b) adhesive strength and (c) energy dissipated by the adhesive material are extracted (Figure S6). Likewise, 180° peel test samples were measured by peeling P3AT films off using adhesive tape (Figure S7). From force−displacement curves, the (d) adhesive peel force (normalized to the width of the tape) was measured relative to the side chain length (Figure S8). (e) Finally, 90° peel tests were performed on glass/PEDOT:PSS/P3AT stacks using adhesive tape, from which the peel force was measured and debonding interface was photographed (Figures S8 and S9). The thickness of the 180° peel test films ranged from 100 to 150 nm in thickness, while the P3AT films used for 90° peel tests were between 300 and 400 nm (Figure S8).

As such, our findings agree with empirical relationships that predict the compressive (bulk) modulus to be greater than the tensile modulus in non-conjugated polymers (Figure S4).[13] We also observed greater agreement between the calculated and measured values of the compressive modulus compared to the tensile modulus (Tables S2 and S4), with the caveat that there was still a significant difference between the two for polymers with glass transitions near room temperature (P3PT, P3HT, and P3HpT, see discussion in the Supporting Information).

From oscillatory indentation measurements, storage modulus (Figures 3a and S5), loss modulus (Figure 3d), and tan δ (Figure 3e) were extracted. Under dynamic conditions, we see significant differences between the loss modulus measured for polymers with glass transition temperatures above and below the operating temperature. Previous work on polycarbonate has shown that the deformation phenomena of the solid film is in part determined by the crazing (deformation resulting from an increase in volume, e.g., formation of void spaces by chain scission or disentanglement) and shear yield (deformation without a change in volume, e.g., chain slippage) transitions.[121,122] Kramer and Berger showed that such transitions are associated with the glass transition temperature, for which the transition between crazing and shear yield occurs approximately 28 °C below T_g for polycarbonate.[121,123] Thus, changes in deformation behavior could possibly provide insight as to the differences between n = 4−5 and n = 6−10 (where there is a monotonic decrease in G''). The damping behavior (tan δ) is calculated as the ratio of the loss and storage (elastic) modulus, for which there was a monotonic increase (from ∼0.05 to ∼0.3) relative to alkyl chain length for n = 4−8. The tan δ is dependent on the operating temperature of the film (here, room temperature) relative to the thermal transitions[48] associated with the polymer film (e.g., glass transition, for which there was a constant decrease as n increased[49]). Our findings were consistent with data reported by the Gu group on the thermal behavior of P3PT and P3HT using dynamic mechanical analysis (DMA) of glass fiber mesh samples.[124] However, the tan δ of P3DT (n = 10) was measured to be 0.2, similar to that of P3HT. This difference is attributed to an increase in the storage modulus (G') (Figures 3a and S5), which possibly stems from an increase in morphological ordering.[54,106,118]

For indentation of all P3AT films, plastic work was greater than elastic work, both under tension (Figure S3) and compression (Figure 3c). The elastic work dissipated increased relative to increasing side chain length, which was counter to the trend observed for resilience under tension (yet similar to that of linear elasticity) (Figure 2c,d). The one outlier was P3OT, which exhibited both the greatest amount of plastic and elastic work. As such, both measurements in tension and in compression suggest that the plastic behavior of P3AT films is dependent, non-monotonically, on the side chain length.

To elucidate the effect of the side chain length on the adhesive properties of P3ATs, lap shear (Figures 4a−c and S6), 180° peel test (Figures 4d,e, S7, and S8), and 90° peel test samples (Figures S8 and S9) were prepared. When subject to shear strain (Figure 4a), an increase in the alkyl chain length generally resulted in an increase in the adhesive strength (Figure 4b) and energy dissipated (Figure 4c, normalized to the surface area of the lap joint). Due to the debonding behavior of P3OT, the total energy dissipated by the lap joint was significantly greater than that of the rest of the P3ATs. These results correlate strongly with the fracture strains and compressive work, in that P3OT has the greatest fracture strain (Figure 2e), total work (Figure 3c) and adhesive strength (Figure 4b). Likewise, the increase in alkyl chain length from n

https://doi.org/10.1021/acs.chemmater.3c00485
Chem. Mater. 2023, 35, 3329−3342

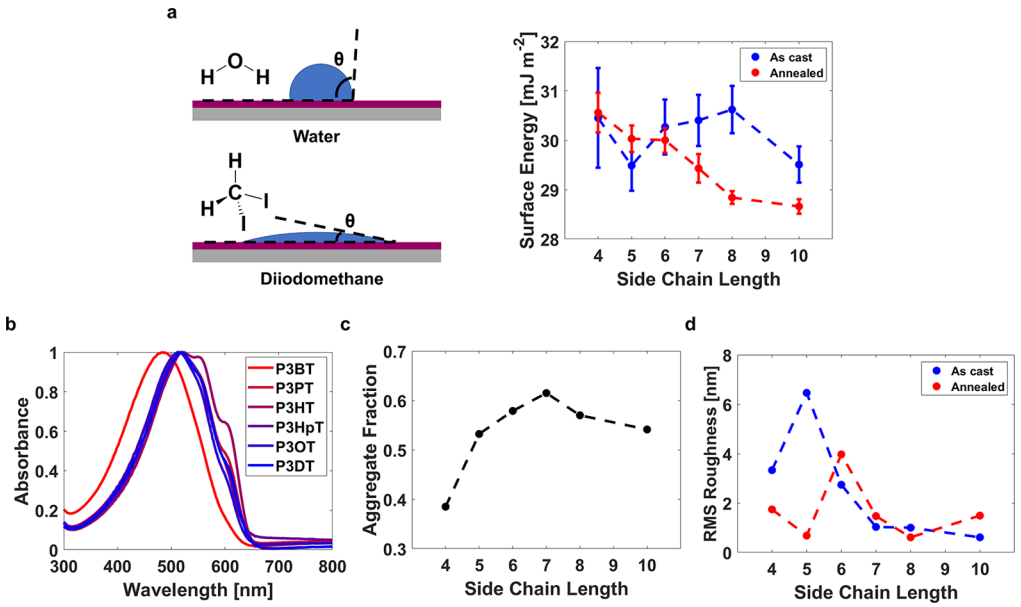

Figure 5. (a) Surface energy measurements of as-cast and annealed (100 °C, 30 min) P3AT films were made using contact angle measurements of water and diiodomethane. (b) UV−vis spectra of P3AT films, from which the (c) aggregate fraction was extracted using a model developed by Spano and coworkers. (d) The mean square roughness for as-cast and annealed P3AT films were measured using AFM (Figure S10).

= 8 to n = 10 resulted in both a decrease in the fracture strain and adhesive strength, suggesting a maximum in the adhesive strength for P3OT.

With an operating temperature significantly below the glass transition, P3BT chains are highly immobile (glassy) at room temperature and thus cannot rearrange to encourage the dissipation of mechanical energy throughout the film. Thus, P3BT (n = 4) films showed the least adhesive strength and displacement (~0.15 mm). P3PT, likewise with a glass transition above the operating temperature, showed a comparable adhesive strength. When the side chain is sufficiently long such that the glass transition is below the operating temperature (n > 5), the polymer film functions as a viscoelastic adhesive between rigid substrates.[125] P3ATs with n = 5−7 and n = 10 all failed with a displacement between 0.5 and 1 mm. However, the maximum load applied was low, suggesting that these polymer films have little resistance to flow.[126] Finally, P3OT showed a clear maximum in adhesive strength, which is likely attributed to the greatest amount of viscoelastic dissipation of energy (as suggested by the relatively high value of tan δ, Figure 3e). The plateau in force relative to increasing displacement (>1 mm) for P3OT suggests that highly mobile polymer chains can undergo significant rearrangement to dissipate the mechanical work (Figure 4a).

Although a clear trend is present from these lap shear measurements, the calculated adhesive strengths of this P3AT library were extremely low (common polymeric adhesives have adhesive strengths on the order of MPa). Our calculations were likely significant underestimates of the actual adhesive strength, as we assume uniformity of the polymer film. Photographs of representative samples (Figure S6) show that the lap joints were primarily held together by a thicker outer border of polymer. A more accurate estimate of the surface area of the adhesive would likely be that corresponding to the thick border of the overlapping lap joint. As such, the calculated adhesive strength should be taken as representative of how these samples were prepared, with more importance being given to the qualitative trend rather than the numerical values. An extended discussion is included in the Supporting Information along with Figure S6 (page S18).

Similar lap shear measurements were conducted on a family of methacrylate-based copolymers with increasing alkyl chain lengths by Payra et al.[127] The authors found a similar maximum when comparing the measured lap shear strength against the glass transition of the synthesized copolymers.[127] Coincidentally, the copolymers with octyl (and 2-ethyl hexyl) side chains also resulted in the greatest lap shear strength (~2.8 MPa). At low glass transitions (T_g ~ −55 to −40 °C), copolymers with decyl and dodecyl side chains were highly ductile, which resulted in mobile polymer chains that yielded easily when subject to low loads (e.g., a low tensile strength but a high fracture strain). In contrast, copolymers with methyl and butyl side chains (T_g ~ −70 to 130 °C) had insufficient ductility due to the glassy nature of the polymer film, which resulted in highly brittle lap joints that, again, failed at low loads once energy storage mechanisms were saturated. Our findings thus suggest that the ability of a conjugated polymer film to function as a lap shear adhesive is dependent on a balance between both a high tensile strength and high fracture strain (as opposed to simply a high toughness, where the strength or ductility could possibly be low).

Additionally, 180° peel tests were conducted to further study the debonding behavior of P3ATs from glass substrates (Figures 4d, S7, and S8). P3BT, with its glassy behavior, required minimal force to delaminate (Figure S7). This behavior corresponds well with the low plasticity and low viscoelasticity (i.e., low tan δ). In contrast, the adhesive peel forces for polymers above their glass transition (n > 5) showed a trend of increasing peel force relative to side chain length (despite random fluctuations in force inherent to the measurement technique[32]), with P3DT again behaving counter to the trend. We observed a maximum around n = 7−8, with P3HpT and P3OT measuring comparable peel forces (Figure 4d). This result agreed with our previous findings, as the progression of the peeling interface results in both tensile and compressive stresses, and depend strongly on the viscoelastic

https://doi.org/10.1021/acs.chemmater.3c00485
Chem. Mater. 2023, 35, 3329−3342

behavior.[32] P3HpT and P3OT films were measured to have the greatest measured toughness (and also plastic dissipation of energy, which is of particular importance to the behavior of the crack growth[128]) under tension and compression, as well as the greatest measured values of tan δ at room temperature (and thus most favorable viscoelastic behavior).

In most envisioned device applications, an applied semiconducting polymer film will likely interface with another transport or sensing layer. In organic solar cells, a polymeric bulk heterojunction is thus often deposited on top of a PEDOT:PSS hole transport layer. We conclude by investigating how an increase in side chain length changes the debonding behavior of a glass/PEDOT:PSS/P3AT/tape stack using 90° peel tests (Figures 4e, S8, and S9). We find that delamination occurs at either the PEDOT:PSS/P3AT (n = 5−7) or P3AT/tape (n = 4, 10) interface, with a transition at n = 8 between the two (Figure S9).

Tuning the side chain structure of a conjugated polymer is a common strategy for optimizing the surface energy of the solid film.[129−131] However, alteration of the ratio of saturated to unsaturated groups within the solid film also potentially affects the surface energy, which would affect the adhesion between two films in contact arising from van der Waals forces.[132] Contact angle measurements were used to determine the effect of the alkyl chain length on the surface energy of the resulting polymer film (Figure 5a). As-cast films showed no coherent trend, with all polymers having an approximate surface energy of ∼30 mJ m^{-2} (although complete elimination of the relatively high-boiling solvent, chlorobenzene, was unlikely without thermal treatment). However, when thermally annealed, the surface energy decreased with increasing side chain length. These findings validate previous results showing that the water contact angle increases for P3AT films of increasing side chain length.[106,133] Annealing removes residual solvent and may also promote the reorientation of the polymer chains into domains with edge-on texture (as previous studies have shown with P3HT).[134,135] Thus, this increase in water contact angle (and decrease in measured surface energy) is attributed to the increased presentation of hydrophobic alkyl side chains at the surface.[133] This observation suggests that the adhesion between the tape and the P3AT film decreases as the side chain length increases, which explains the debonding behavior shown in the 90° peel tests (Figure S9).

The greatest peel force was measured for P3BT (∼120 N m^{-1}), which delaminated at the P3BT/tape interface. While the high surface energy allowed for the best adhesion between the tape and polymer film, the high stiffness and strength of the film likely prevented bending, and thus fracture from propagating throughout the film. The mechanical properties of the PEDOT:PSS layer also likely contributed to this observed debonding behavior. P3BT was the only polymer in the series to have an elastic modulus greater than PEDOT:PSS (∼385 MPa[136]), which likely prevented crazing at the PEDOT:PSS/P3BT interface due to elastic mismatch. In contrast, n = 5−7 all delaminated at the PEDOT:PSS/P3AT interface with low measured peel forces (∼60 N m^{-1}), which is consistent with findings from the Dauskardt group showing that the PEDOT:PSS/P3HT:PCBM interface is weakest within a device stack.[42,84] At n = 8, there was a transition at which the adhesion between the P3AT/tape interface became weak enough such that it becomes the most favorable debonding interface. However, at this transition, the PEDOT:PSS/P3OT interface was still weak enough to delaminate, resulting in debonding occurring at both interfaces (Figure S8b). This meandering fracture path,[86] as well as the formation of four new surfaces rather than two, likely resulted in a relatively high measured peel force (∼110 N m^{-1}). Finally, for P3DT, the P3DT/tape interface was clearly the weakest due to the poor adhesion between the two; the same amount of force needed to delaminate the P3AT film from PEDOT:PSS for n = 5−7 is sufficient to peel tape off the P3DT film. As such, these findings suggest that the length (and structure) of the side chain play a significant role in determining the fracture behavior of a device stack which incorporates a conjugated polymer film. Likewise, the mechanical properties of the P3AT film (as well as the adjacent layers) govern how debonding occurs and how the fracture tip propagates. For example, both P3BT and P3DT delaminated at the P3AT/tape interface, yet for different reasons.

Finally, the aggregation and topography of the P3AT films were characterized using UV−vis (Figure 5b,c) and AFM (Figures 5d and S10) to determine their effects on the observed mechanical behaviors. A comparison of the measured aggregate fraction to the degree of polymerization showed no apparent trend (Figure S11). P3BT had the lowest aggregation (∼0.4), likely due to the kinetically frozen structure preventing the formation of aggregates, while all other P3ATs had aggregate fractions above 0.5. Interestingly, P3HpT had the greatest fraction of aggregates, which possibly contributed to the significant plastic deformation (e.g., energy dissipated due to the breaking of aggregates) and relatively high fracture strain observed from FOW measurements. Likewise, AFM phase images were used to investigate the topography of P3AT films (Figure S10), from which the root-mean roughness are extracted (Figure 5d), as the adhesion is additionally dependent on the contact area between two surfaces (and thus, the roughness and topography of each surface).[137−139] For example, an increased surface roughness can improve mechanical adhesion by allowing for the interlocking of the two surfaces,[140,141] or significantly reduce adhesion when an elastic solid (e.g., rubber) is in contact with a hard substrate.[142] However, the P3AT films used in this study were similar in surface roughness, and thus not likely to have significantly affected the measurements performed.

■ CONCLUSIONS

Here, we sought to understand how the length of the alkyl chain side chain affects the mechanical and adhesive properties of a library of poly(3-alkylthiophene) (P3AT) films using four methods: a quasi-free-standing tensile test, compressive nanoindentation, a lap-joint shear test, and adhesive peel tests. We find that the length of the alkyl side chain significantly impacts the elastic storage of energy, plastic dissipation of energy, and surface energy. While elastic properties have a relatively monotonic relationship relative to side chain length, plastic properties are typically non-monotonic. These relationships between mechanical behavior (and electronic performance) and side chain length govern the viscoelasticity of the P3AT film. At a specific operating temperature (here, room temperature), the bulk (e.g., viscoelasticity, plasticity, and elasticity) and surface (e.g., viscoelasticity and surface energy) properties govern the ability of the polymer film to function as an ersatz adhesive within a device stack. For poly(3-alkylthiophene) thin films, we find that the most favorable mechanical properties for stretchable

https://doi.org/10.1021/acs.chemmater.3c00485
Chem. Mater. 2023, 35, 3329−3342

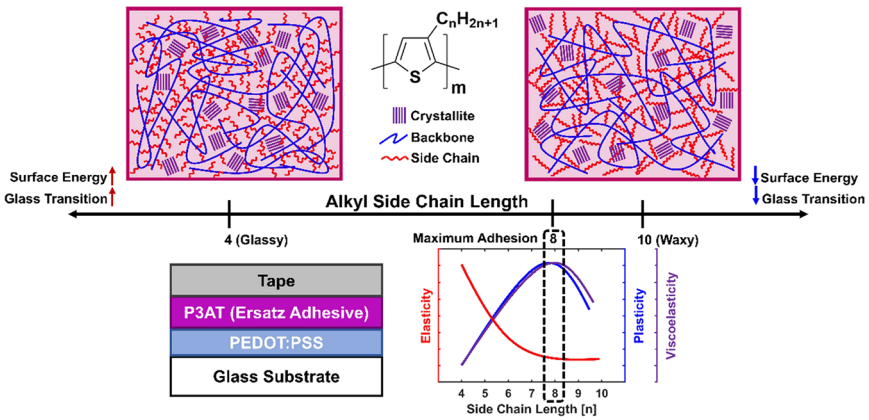

Figure 6. Summary of changes in the morphology and mechanical behavior in poly(3-alkylthiophene) thin films as the side chain length increases from $n = 4$ to $n = 10$. These monotonic and non-monotonic relationships govern the functionality of the semiconducting polymer film to function as an ersatz adhesive within a device stack.

and soft electronics occur with a side chain length of $n = 7$ (P3HpT) or $n = 8$ (P3OT). Similarly, the increase in side chain length results in an relatively monotonic tradeoff between increasing deformability ("softness") and decreasing surface energy. As a result, P3OT displays the best adhesive functionality, both as a viscoelastic adhesive gluing together two glass slides and as a polymeric interlayer in an example device stack (e.g., when deposited on top of PEDOT:PSS). We summarize our findings below (Figure 6).

The envisioned application of semiconducting polymers in flexible and stretchable electronics is dependent on the electronic, mechanical, and adhesive performance, which often have tradeoffs that must be optimized. Here, we demonstrate how methods common to conventional polymers can be used to characterize the mechanical behavior of semiconducting polymers in detail in order to understand these tradeoffs. While our study only evaluates the effect of side chain length on one model family of conjugated polymers (i.e., poly(3-alkylthiophene)), the backbone structure is also a significant determinant of the mechanical and adhesive properties of the solid polymer film. Likewise, while most conjugated polymers still feature linear or branched alkyl side chains, the chemical structure can be rationally designed to improve the mechanical and adhesive performance of the polymer film (functionalization of the side chain with, e.g., amines, catechol, hydrogen bonding moieties) within a device stack. Additionally, semiconducting polymers are applied in a broad range of device applications, and thus interface with many types of sensing, transport, and electrode materials. The adhesive and debonding behavior of many of these interfaces are seldom explored, and offer opportunities for improving the mechanical robustness and stability of these devices. For example, the interface of the lap-joint shear samples can be changed (e.g., by depositing PEDOT:PSS on top of the glass substrates) in order to investigate interfaces more relevant to device stacks. Finally, empirical correlations have been developed to relate chemical and molecular structure to elastic modulus in conventional (non-conjugated) polymers, but these correlations do not apply well to conjugated polymers, particularly those operating at a temperature where both glassy and rubbery behavior is demonstrated. As such, our findings motivate further study of how the different electronic, mechanical, and adhesive figures of merit can be tuned be systematically tuned by rational design of the polymer structure.

■ ASSOCIATED CONTENT

Supporting Information

The Supporting Information is available free of charge at https://pubs.acs.org/doi/10.1021/acs.chemmater.3c00485.

Experimental methods; theoretical calculations and discussion; molecular weight, dispersity, and regioregularity of polymers; values of calculated moduli and supplementary figures; photographs of samples; AFM characterization (PDF)

■ AUTHOR INFORMATION

Corresponding Author

Darren J. Lipomi − *Department of Nanoengineering, University of California, La Jolla, California 92093, United States;* orcid.org/0000-0002-5808-7765; Email: dlipomi@ucsd.edu

Authors

Alexander X. Chen − *Department of Nanoengineering, University of California, La Jolla, California 92093, United States;* orcid.org/0000-0003-1919-6755

Silpa S. Pazhankave − *School of Sustainable Engineering and the Built Environment, Arizona State University, Tempe, Arizona 85287, United States*

Jordan A. Bunch − *Department of Nanoengineering, University of California, La Jolla, California 92093, United States*

Allison Lim − *Department of Nanoengineering, University of California, La Jolla, California 92093, United States*

Kartik Choudhary − *Department of Nanoengineering, University of California, La Jolla, California 92093, United States;* orcid.org/0000-0003-2611-8982

Guillermo L. Esparza − *Department of Nanoengineering, University of California, La Jolla, California 92093, United States; Materials Science and Engineering Program, University of California, La Jolla, California 92093, United States*

Rory Runser − *Department of Nanoengineering, University of California, La Jolla, California 92093, United States*

https://doi.org/10.1021/acs.chemmater.3c00485
Chem. Mater. 2023, 35, 3329−3342

Christian G. Hoover − *School of Sustainable Engineering and the Built Environment, Arizona State University, Tempe, Arizona 85287, United States*

Complete contact information is available at: https://pubs.acs.org/10.1021/acs.chemmater.3c00485

Notes

The authors declare no competing financial interest.

■ ACKNOWLEDGMENTS

This work was supported by the Air Force Office of Scientific Research (AFOSR) grant no. FA9550-22-1-0454 to D.J.L. A.X.C. acknowledges support from the UC President's Dissertation Year Fellowship. S.S.P. and C.G.H. acknowledge financial support from the Zimin Institute for Smart and Sustainable Cities at ASU under award no. AWD00034680. The authors acknowledge the use of facilities and instrumentation supported by NSF through the UC San Diego Materials Research Science and Engineering Center (UCSD MRSEC), grant DMR-2011924. This work was performed in part at the San Diego Nanotechnology Infrastructure (SDNI) of UC San Diego, a member of the National Nanotechnology Coordinated Infrastructure, which is supported by the National Science Foundation (Grant ECCS-2025752). The authors would like to thank Ricardo De-luna for support with the GPC measurements and Prof. Shengqiang Cai for helpful discussions.

■ REFERENCES

(1) Kayser, L. V.; Lipomi, D. J. Stretchable Conductive Polymers and Composites Based on PEDOT and PEDOT:PSS. *Adv. Mater.* **2019**, *31*, No. 1806133.
(2) Lee, C.; Lee, S.; Kim, G. U.; Lee, W.; Kim, B. J. Recent Advances, Design Guidelines, and Prospects of All-Polymer Solar Cells. *Chem. Rev.* **2019**, *119*, 8028−8086.
(3) Someya, T.; Bao, Z.; Malliaras, G. G. The Rise of Plastic Bioelectronics. *Nature* **2016**, *540*, 379−385.
(4) Heeger, A. J. Semiconducting Polymers: The Third Generation. *Chem. Soc. Rev.* **2010**, *39*, 2354−2371.
(5) Forrest, S. R.; Thompson, M. E. Introduction: Organic Electronics and Optoelectronics. *Chem. Rev.* **2007**, *107*, 923−925.
(6) Khau, B. V.; Scholz, A. D.; Reichmanis, E. Advances and Opportunities in Development of Deformable Organic Electrochemical Transistors. *J. Mater. Chem. C* **2020**, *8*, 15067−15078.
(7) Liang, Y.; Wu, Y.; Feng, D.; Tsai, S. T.; Son, H. J.; Li, G.; Yu, L. Development of New Semiconducting Polymers for High Performance Solar Cells. *J. Am. Chem. Soc.* **2009**, *131*, 56−57.
(8) Liang, Y.; Yu, L. A New Class of Semiconducting Polymers for Bulk Heterojunction Solar Cells with Exceptionally High Performance. *Acc. Chem. Res.* **2010**, *43*, 1227−1236.
(9) Lee, G. H.; Moon, H.; Kim, H.; Lee, G. H.; Kwon, W.; Yoo, S.; Myung, D.; Yun, S. H.; Bao, Z.; Hahn, S. K. Multifunctional Materials for Implantable and Wearable Photonic Healthcare Devices. *Nat. Rev. Mater.* **2020**, *5*, 149−165.
(10) Root, S. E.; Savagatrup, S.; Printz, A. D.; Rodriquez, D.; Lipomi, D. J. Mechanical Properties of Organic Semiconductors for Stretchable, Highly Flexible, and Mechanically Robust Electronics. *Chem. Rev.* **2017**, *117*, 6467−6499.
(11) Nielsen, L. E.; Landel, R. F. *Mechanical Properties of Polymers and Composites*, 2nd edition; CRC Press, 1993.
(12) Cooper, A. R. Mechanical Properties of Polymers: The Influence of Molecular Weight and Molecular Weight Distribution. *J. Macromol. Sci. C* **1972**, *8*, 57−199.
(13) Seitz, J. T. The Estimation of Mechanical Properties of Polymers from Molecular Structure. *J. Appl. Polym. Sci.* **1993**, *49*, 1331−1351.
(14) Chen, A. X.; Hilgar, J. D.; Samoylov, A. A.; Pazhankave, S. S.; Bunch, J. A.; Choudhary, K.; Esparza, G. L.; Lim, A.; Luo, X.; Chen, H.; Runser, R.; Mcculloch, I.; Mei, J.; Hoover, C.; Printz, A. D.; Romero, N. A.; Lipomi, D. J. Increasing the Strength, Hardness, and Survivability of Semiconducting Polymers by Crosslinking. *ACS Appl. Mater. Interfaces* **2023**, *10*, No. 2202503.
(15) Wang, Z.; Zhang, D.; Xu, M.; Liu, J.; He, J.; Yang, L.; Li, Z.; Gao, Y.; Shao, M. Intrinsically Stretchable Organic Solar Cells with Simultaneously Improved Mechanical Robustness and Morphological Stability Enabled by a Universal Crosslinking Strategy. *Small* **2022**, *18*, No. 2201589.
(16) Kim, M. J.; Lee, M.; Min, H.; Kim, S.; Yang, J.; Kweon, H.; Lee, W.; Kim, D. H.; Choi, J. H.; Ryu, D. Y.; Kang, M. S.; Kim, B. S.; Cho, J. H. Universal Three-Dimensional Crosslinker for All-Photopatterned Electronics. *Nat. Commun.* **2020**, *11*, 1520.
(17) Rumer, J. W.; McCulloch, I. Organic Photovoltaics: Crosslinking for Optimal Morphology and Stability. *Mater. Today* **2015**, *18*, 425−435.
(18) Zheng, Y.; Yu, Z.; Zhang, S.; Kong, X.; Michaels, W.; Wang, W.; Chen, G.; Liu, D.; Lai, J.; Prine, N.; Zhang, W.; Nikzad, S.; Cooper, C. B.; Zhong, D.; Mun, J.; Zhang, Z.; Kang, J.; Tok, J. B.; Mcculloch, I.; Qin, J.; Gu, X.; Bao, Z. A Molecular Design Approach towards Elastic and Multifunctional Polymer Electronics. *Nat. Commun.* **2021**, *12*, 5701.
(19) Xu, J.; Wang, S.; Wang, G. N.; Zhu, C.; Luo, S.; Jin, L.; Gu, X.; Chen, S.; Feig, V. R.; To, J. W. F.; Rondeau-gagné, S.; Park, J.; Schroeder, B. C.; Lu, C.; Oh, J. Y.; Wang, Y.; Kim, Y.; Yan, H.; Sinclair, R.; Zhou, D.; Xue, G.; Murmann, B.; Linder, C.; Cai, W.; Tok, J. B. Highly Stretchable Polymer Semiconductor Films through the Nanoconfinement Effect. 2017, *355*, 59−64, DOI: 10.1126/science.aah4496.
(20) Wang, S.; Xu, J.; Wang, W.; Wang, G. J. N.; Rastak, R.; Molina-Lopez, F.; Chung, J. W.; Niu, S.; Feig, V. R.; Lopez, J.; Lei, T.; Kwon, S. K.; Kim, Y.; Foudeh, A. M.; Ehrlich, A.; Gasperini, A.; Yun, Y.; Murmann, B.; Tok, J. B. H.; Bao, Z. Skin Electronics from Scalable Fabrication of an Intrinsically Stretchable Transistor Array. *Nature* **2018**, *555*, 83−88.
(21) Xu, J.; Wu, H. C.; Zhu, C.; Ehrlich, A.; Shaw, L.; Nikolka, M.; Wang, S.; Molina-Lopez, F.; Gu, X.; Luo, S.; Zhou, D.; Kim, Y. H.; Wang, G. J. N.; Gu, K.; Feig, V. R.; Chen, S.; Kim, Y.; Katsumata, T.; Zheng, Y. Q.; Yan, H.; Chung, J. W.; Lopez, J.; Murmann, B.; Bao, Z. Multi-Scale Ordering in Highly Stretchable Polymer Semiconducting Films. *Nat. Mater.* **2019**, *18*, 594−601.
(22) Melenbrink, E. L.; Hilby, K. M.; Choudhary, K.; Samal, S.; Kazerouni, N.; McConn, J. L.; Lipomi, D. J.; Thompson, B. C. Influence of Acceptor Side-Chain Length and Conjugation-Break Spacer Content on the Mechanical and Electronic Properties of Semi-Random Polymers. *ACS Appl. Polym. Mater.* **2019**, *1*, 1107−1117.
(23) Sugiyama, F.; Kleinschmidt, A. T.; Kayser, L. V.; Alkhadra, M. A.; Wan, J. M. H.; Chiang, A. S. C.; Rodriquez, D.; Root, S. E.; Savagatrup, S.; Lipomi, D. J. Stretchable and Degradable Semiconducting Block Copolymers. *Macromolecules* **2018**, *51*, 5944−5949.
(24) Lee, Y.; Oh, J. Y.; Xu, W.; Kim, O.; Kim, T. R.; Kang, J.; Kim, Y.; Son, D.; Tok, J. B. H.; Park, M. J.; Bao, Z.; Lee, T. W. Stretchable Organic Optoelectronic Sensorimotor Synapse. *Sci. Adv.* **2018**, *4*, No. eaat7387.
(25) Printz, A. D.; Savagatrup, S.; Burke, D. J.; Purdy, T. N.; Lipomi, D. J. Increased Elasticity of a Low-Bandgap Conjugated Copolymer by Random Segmentation for Mechanically Robust Solar Cells. *RSC Adv.* **2014**, *4*, 13635−13643.
(26) Müller, C.; Goffri, S.; Breiby, D. W.; Andreasen, J. W.; Chanzy, H. D.; Janssen, R. A. J.; Nielsen, M. M.; Radano, C. P.; Sirringhaus, H.; Smith, P.; Stingelin-Stutzmann, N. Tough, Semiconducting Polyethylene-Poly(3-Hexylthiophene) Diblock Copolymers. *Adv. Funct. Mater.* **2007**, *17*, 2674−2679.
(27) Zokaei, S.; Kroon, R.; Gladisch, J.; Paulsen, B. D.; Sohn, W.; Hofmann, A. I.; Persson, G.; Stamm, A.; Syrén, P. O.; Olsson, E.; Rivnay, J.; Stavrinidou, E.; Lund, A.; Müller, C. Toughening of a Soft

Polar Polythiophene through Copolymerization with Hard Urethane Segments. *Adv. Sci.* **2021**, *8*, No. 2002778.
(28) Kayser, L. V.; Russell, M. D.; Rodriquez, D.; Abuhamdieh, S. N.; Dhong, C.; Khan, S.; Stein, A. N.; Ramírez, J.; Lipomi, D. J. RAFT Polymerization of an Intrinsically Stretchable Water-Soluble Block Copolymer Scaffold for PEDOT. *Chem. Mater.* **2018**, *30*, 4459−4468.
(29) Seo, S.; Lee, J.-W.; Kim, D. J.; Lee, D.; Phan, T. N.-L.; Park, J.; Tan, Z.; Cho, S.; Kim, T.-S.; Kim, B. J. Poly(Dimethylsiloxane)-Block-PM6 Polymer Donors for High-Performance and Mechanically-Robust Polymer Solar Cells. *Adv. Mater.* **2023**, No. 2300230.
(30) Park, S. H.; Kim, Y.; Kwon, N. Y.; Lee, Y. W.; Woo, H. Y.; Chae, W. S.; Park, S.; Cho, M. J.; Choi, D. H. Significantly Improved Morphology and Efficiency of Nonhalogenated Solvent-Processed Solar Cells Derived from a Conjugated Donor−Acceptor Block Copolymer. *Adv. Sci.* **2020**, *7*, No. 1902470.
(31) Park, H.; Ma, B. S.; Kim, J.; Kim, Y.; Kim, H. J.; Kim, D.; Yun, H.; Han, J.; Kim, F. S.; Kim, T.; Kim, B. J. Regioregular- Block -Regiorandom Poly(3-Hexylthiophene) Copolymers for Mechanically Robust and High-Performance Thin- Film Transistors. *Macromolecules* **2019**, *52*, 7721−7730.
(32) Wu, S. *Polymer Interface and Adhesion*, 1st edition; Taylor & Francis, 1982.
(33) Wang, Z.; Wang, W.; Wang, S. Surface Adhesion Engineering for Robust Organic Semiconductor Devices. *J. Mater. Chem. C* **2022**, *10*, 2516−2526.
(34) Wake, W. C. Theories of Adhesion and Uses of Adhesives: A Review. *Polymer* **1978**, *19*, 291−308.
(35) Creton, C.; Ciccotti, M. Fracture and Adhesion of Soft Materials: A Review. *Rep. Prog. Phys.* **2016**, *79*, No. 046601.
(36) Mittal, K. L. The Role of the Interface in Adhesion Phenomena. *Polym. Eng. Sci.* **1977**, *17*, 467−473.
(37) Derjaguin, B. V.; Smilga, V. P. Electronic Theory of Adhesion. *J. Appl. Phys.* **1967**, *38*, 4609−4616.
(38) Feldstein, M. M.; Siegel, R. A. Molecular and Nanoscale Factors Governing Pressure-Sensitive Adhesion Strength of Viscoelastic Polymers. *J. Polym. Sci. B Polym. Phys.* **2012**, *50*, 739−772.
(39) Godwin, A. D. Plasticizers. In *Applied Plastics Engineering Handbook*; William Andrew, 2017; pp. 533−553.
(40) Moore, D. F.; Geyer, W. A Review of Adhesion Theories for Elastomers. *Wear* **1972**, *22*, 113−141.
(41) Bruner, C.; Dauskardt, R. Role of Molecular Weight on the Mechanical Device Properties of Organic Polymer Solar Cells. *Macromolecules* **2014**, *47*, 1117−1121.
(42) Brand, V.; Bruner, C.; Dauskardt, R. H. Cohesion and Device Reliability in Organic Bulk Heterojunction Photovoltaic Cells. *Sol. Energy Mater. Sol. Cells* **2012**, *99*, 182−189.
(43) Kinloch, A. J.; Lau, C. C.; Williams, J. G. The Peeling of Flexible Laminates. *Int. J. Fract.* **1994**, *66*, 45−70.
(44) Wei, Y.; Hutchinson, J. W. Interface Strength, Work of Adhesion and Plasticity in the Peel Test. *Int. J. Fract.* **1998**, *93*, 315−333.
(45) Thouless, M. D.; Jensen, H. M. Elastic Fracture Mechanics of the Peel-Test Geometry. *J. Adhes.* **1992**, *38*, 185−197.
(46) Finn, M.; Martens, C. J.; Zaretski, A. V.; Roth, B.; Søndergaard, R. R.; Krebs, F. C.; Lipomi, D. J. Mechanical Stability of Roll-to-Roll Printed Solar Cells under Cyclic Bending and Torsion. *Sol. Energy Mater. Sol. Cells* **2018**, *174*, 7−15.
(47) Postema, A. R.; Liou, K.; Wudl, F.; Smith, P. Highly Oriented, Low-Modulus Materials from Liquid Crystalline Polymers: The Ultimate Penalty for Solubilizing Alkyl Side Chains. *Macromolecules* **1990**, *23*, 1842−1845.
(48) Balar, N.; Siddika, S.; Kashani, S.; Peng, Z.; Rech, J. J.; Ye, L.; You, W.; Ade, H.; O'Connor, B. T. Role of Secondary Thermal Relaxations in Conjugated Polymer Film Toughness. *Chem. Mater.* **2020**, *32*, 6540−6549.
(49) Müller, C. On the Glass Transition of Polymer Semiconductors and Its Impact on Polymer Solar Cell Stability. *Chem. Mater.* **2015**, *27*, 2740−2754.
(50) Qian, Z.; Cao, Z.; Galuska, L.; Zhang, S.; Xu, J.; Gu, X. Glass Transition Phenomenon for Conjugated Polymers. *Macromol. Chem. Phys.* **2019**, *220*, No. 1900062.
(51) Savagatrup, S.; Printz, A. D.; Rodriquez, D.; Lipomi, D. J. Best of Both Worlds: Conjugated Polymers Exhibiting Good Photovoltaic Behavior and High Tensile Elasticity. *Macromolecules* **2014**, *47*, 1981−1992.
(52) Savagatrup, S.; Printz, A. D.; Wu, H.; Rajan, K. M.; Sawyer, E. J.; Zaretski, A. V.; Bettinger, C. J.; Lipomi, D. J. Viability of Stretchable Poly(3-Heptylthiophene) (P3HpT) for Organic Solar Cells and Field-Effect Transistors. *Synth. Met.* **2015**, *203*, 208−214.
(53) Pankaj, S.; Beiner, M. Confined Dynamics and Crystallization in Self-Assembled Alkyl Nanodomains. *J. Phys. Chem. B* **2010**, *114*, 15459−15465.
(54) Pankaj, S.; Hempel, E.; Beiner, M. Side-Chain Dynamics and Crystallization in a Series of Regiorandom Poly(3-Alkylthiophenes). *Macromolecules* **2009**, *42*, 716−724.
(55) Sharma, A.; Pan, X.; Bjuggren, J. M.; Gedefaw, D.; Xu, X.; Kroon, R.; Wang, E.; Campbell, J. A.; Lewis, D. A.; Andersson, M. R. Probing the Relationship between Molecular Structures, Thermal Transitions, and Morphology in Polymer Semiconductors Using a Woven Glass-Mesh-Based DMTA Technique. *Chem. Mater.* **2019**, *31*, 6740−6749.
(56) Balar, N.; Rech, J. J.; Siddika, S.; Song, R.; Schrickx, H. M.; Sheikh, N.; Ye, L.; Megret Bonilla, A.; Awartani, O.; Ade, H.; You, W.; O'Connor, B. T. Resolving the Molecular Origin of Mechanical Relaxations in Donor−Acceptor Polymer Semiconductors. *Adv. Funct. Mater.* **2022**, *32*, No. 2105597.
(57) Mei, J.; Bao, Z. Side Chain Engineering in Solution-Processable Conjugated Polymers. *Chem. Mater.* **2014**, *26*, 604−615.
(58) Rodriquez, D.; Kohl, J. G.; Morel, P.; Burrows, K.; Favaro, G.; Root, S. E.; Ramírez, J.; Alkhadra, M. A.; Carpenter, C. W.; Fei, Z.; Boufflet, P.; Heeney, M.; Lipomi, D. J. Measurement of Cohesion and Adhesion of Semiconducting Polymers by Scratch Testing: Effect of Side-Chain Length and Degree of Polymerization. *ACS Macro Lett.* **2018**, *7*, 1003−1009.
(59) Rodriquez, D.; Kim, J.; Root, S. E.; Fei, Z.; Bou, P.; Heeney, M.; Kim, T.; Lipomi, D. J. Comparison of Methods for Determining the Mechanical Properties of Semiconducting Polymer Films for Stretchable Electronics. *ACS Appl. Mater. Interfaces* **2017**, *9*, 8855−8862.
(60) Printz, A. D.; Zaretski, A. V.; Savagatrup, S.; Chiang, A. S.; Lipomi, D. J. Yield Point of Semiconducting Polymer Films on Stretchable Substrates Determined by Onset of Buckling. *ACS Appl. Mater. Interfaces* **2015**, *7*, 23257−23264.
(61) Stafford, C. M.; Harrison, C.; Beers, K. L.; Karim, A.; Amis, E. J.; Vanlandingham, M. R.; Kim, H. C.; Volksen, W.; Miller, R. D.; Simonyi, E. E. A Buckling-Based Metrology for Measuring the Elastic Moduli of Polymeric Thin Films. *Nat. Mater.* **2004**, *3*, 545−550.
(62) Kim, J.; Nizami, A.; Hwangbo, Y.; Jang, B.; Lee, H.; Woo, C.; Hyun, S.; Kim, T. Tensile Testing of Ultra-Thin Films on Water Surface. *Nat. Commun.* **2013**, *4*, 2520.
(63) Chen, A. X.; Kleinschmidt, A. T.; Choudhary, K.; Lipomi, D. J. Beyond Stretchability: Strength, Toughness, and Elastic Range in Semiconducting Polymers. *Chem. Mater.* **2020**, *32*, 7582−7601.
(64) Yoshino, K.; Morita, S.; Uchida, M.; Muro, K.; Kawai, T.; Ohmori, Y. Novel Electrical and Optical Properties of Poly(3-Alkylthiophene) as Function of Alkyl Chain Length and Their Functional Applications. *Synth. Met.* **1993**, *55*, 28−35.
(65) Ohmori, Y.; Uchida, M.; Muro, K.; Yoshino, K. Effects of Alkyl Chain Length and Carrier Confinement Layer on Characteristics of Poly(3-Alkylthiophene) Electroluminescent Diodes. *Solid State Commun.* **1991**, *80*, 605−608.
(66) Yoshino, K.; Manda, Y.; Sawada, K.; Onoda, M.; Sugimoto, R. I. Anomalous Dependences of Luminescence of Poly(3-Alkylthiophene) on Temperature and Alkyl Chain Length. *Solid State Commun.* **1989**, *69*, 143−146.
(67) Thankaraj Salammal, S.; Dai, S.; Pietsch, U.; Grigorian, S.; Koenen, N.; Scherf, U.; Kayunkid, N.; Brinkmann, M. Influence of

https://doi.org/10.1021/acs.chemmater.3c00485
Chem. Mater. 2023, 35, 3329−3342

Alkyl Side Chain Length on the In-Plane Stacking of Room Temperature and Low Temperature Cast Poly(3-Alkylthiophene) Thin Films. *Eur. Polym. J.* **2015**, *67*, 199−212.
(68) Park, Y. D.; Kim, D. H.; Jang, Y.; Cho, J. H.; Hwang, M.; Lee, H. S.; Lim, J. A.; Cho, K. Effect of Side Chain Length on Molecular Ordering and Field-Effect Mobility in Poly(3-Alkylthiophene) Transistors. *Org. Electron.* **2006**, *7*, 514−520.
(69) Sauvé, G.; Javier, A. E.; Zhang, R.; Liu, J.; Sydlik, S. A.; Kowalewski, T.; McCullough, R. D. Well-Defined, High Molecular Weight Poly(3-Alkylthiophene)s in Thin-Film Transistors: Side Chain Invariance in Field-Effect Mobility. *J. Mater. Chem.* **2010**, *20*, 3195−3201.
(70) Babel, A.; Jenekhe, S. A. Alkyl Chain Length Dependence of the Field-Effect Carrier Mobility in Regioregular Poly(3-Alkylthiophene)-S. *Synth. Met.* **2005**, *148*, 169−173.
(71) Kaneto, K.; Lim, W. Y.; Takashima, W.; Endo, T.; Rikukawa, M. Alkyl Chain Length Dependence of Field-Effect Mobilities in Regioregular Poly(3-Alkylthiophene) Films. *Jpn. J. Appl. Phys.* **2000**, *39*, L872.
(72) Lee, H. S.; Cho, J. H.; Cho, K.; Park, Y. D. Alkyl Side Chain Length Modulates the Electronic Structure and Electrical Characteristics of Poly(3-Alkylthiophene) Thin Films. *J. Phys. Chem. C* **2013**, *117*, 11764−11769.
(73) O'Connor, T. F.; Zaretski, A. V.; Shiravi, B. A.; Savagatrup, S.; Printz, A. D.; Diaz, M. I.; Lipomi, D. J. Stretching and Conformal Bonding of Organic Solar Cells to Hemispherical Surfaces. *Energy Environ. Sci.* **2014**, *7*, 370−378.
(74) Oosterbaan, W. D.; Bolsée, J. C.; Gadisa, A.; Vrindts, V.; Bertho, S.; D'Haen, J.; Cleij, T. J.; Lutsen, L.; McNeill, C. R.; Thomsen, L.; Manca, J. V.; Vanderzande, D. Alkyl-Chain-Length-Independent Hole Mobility via Morphological Control with Poly(3-Alkylthiophene) Nanofibers. *Adv. Funct. Mater.* **2010**, *20*, 792−802.
(75) Nguyen, L. H.; Hoppe, H.; Erb, T.; Günes, S.; Gobsch, G.; Sariciftci, N. S. Effects of Annealing on the Nanomorphology and Performance of Poly(Alkylthiophene):Fullerene Bulk-Heterojunction Solar Cells. *Adv. Funct. Mater.* **2007**, *17*, 1071−1078.
(76) Liu, Y.; Xian, K.; Gui, R.; Zhou, K.; Liu, J.; Gao, M.; Zhao, W.; Jiao, X.; Deng, Y.; Yin, H.; Geng, Y.; Ye, L. Simple Polythiophene Solar Cells Approaching 10% Efficiency via Carbon Chain Length Modulation of Poly(3-Alkylthiophene). *Macromolecules* **2022**, *55*, 133−145.
(77) Zheng, C.; Jalan, I.; Cost, P.; Oliver, K.; Gupta, A.; Misture, S.; Cody, J. A.; Collison, C. J. Impact of Alkyl Chain Length on Small Molecule Crystallization and Nanomorphology in Squaraine-Based Solution Processed Solar Cells. *J. Phys. Chem. C* **2017**, *121*, 7750−7760.
(78) Cho, C. H.; Kim, H. J.; Kang, H.; Shin, T. J.; Kim, B. J. The Effect of Side-Chain Length on Regioregular Poly[3-(4-n-Alkyl) Phenylthiophene]/PCBM and ICBA Polymer Solar Cells. *J. Mater. Chem.* **2012**, *22*, 14236−14245.
(79) Huang, W. Y.; Lee, C. C.; Wang, S. G.; Han, Y. K.; Chang, M. Y. Side Chain Effects of Poly(3-Alkylthiophene) on the Morphology and Performance of Polymer Solar Cells. *J. Electrochem. Soc.* **2010**, *157*, B1336.
(80) Friedel, B.; McNeill, C. R.; Greenham, N. C. Influence of Alkyl Side-Chain Length on the Performance of Poly(3-Alkylthiophene)/Polyfluorene All-Polymer Solar Cells. *Chem. Mater.* **2010**, *22*, 3389−3398.
(81) Li, C.; Zhu, R.; Lai, J.; Tan, J.; Luo, Y.; Ye, S. Conformational Order of Alkyl Side Chain of Poly(3-Alkylthiophene) Promotes Hole-Extraction Ability in Perovskite/Poly(3-Alkylthiophene) Heterojunction. *J. Phys. Chem. Lett.* **2021**, *12*, 11817−11823.
(82) Bruner, C.; Novoa, F.; Dupont, S.; Dauskardt, R. Decohesion Kinetics in Polymer Organic Solar Cells. *ACS Appl. Mater. Interfaces* **2014**, *6*, 21474−21483.
(83) Dupont, S. R.; Voroshazi, E.; Heremans, P.; Dauskardt, R. H. Adhesion Properties of Inverted Polymer Solarcells: Processing and Film Structure Parameters. *Org. Electron. Phys. Mater. Appl.* **2013**, *14*, 1262−1270.
(84) Dupont, S. R.; Oliver, M.; Krebs, F. C.; Dauskardt, R. H. Interlayer Adhesion in Roll-to-Roll Processed Flexible Inverted Polymer Solar Cells. *Sol. Energy Mater. Sol. Cells* **2012**, *97*, 171−175.
(85) Lee, I.; Rolston, N.; Brunner, P. L.; Dauskardt, R. H. Hole-Transport Layer Molecular Weight and Doping Effects on Perovskite Solar Cell Efficiency and Mechanical Behavior. *ACS Appl. Mater. Interfaces* **2019**, *11*, 23757−23764.
(86) Watson, B. L.; Rolston, N.; Printz, A. D.; Dauskardt, R. H. Scaffold-Reinforced Perovskite Compound Solar Cells. *Energy Environ. Sci.* **2017**, *10*, 2500−2508.
(87) Rolston, N.; Watson, B. L.; Bailie, C. D.; McGehee, M. D.; Bastos, J. P.; Gehlhaar, R.; Kim, J. E.; Vak, D.; Mallajosyula, A. T.; Gupta, G.; Mohite, A. D.; Dauskardt, R. H. Mechanical Integrity of Solution-Processed Perovskite Solar Cells. *Extrem. Mech. Lett.* **2016**, *9*, 353−358.
(88) Choi, J.; Kim, W.; Kim, S.; Kim, T. S.; Kim, B. J. Influence of Acceptor Type and Polymer Molecular Weight on the Mechanical Properties of Polymer Solar Cells. *Chem. Mater.* **2019**, *31*, 9057−9069.
(89) Dupont, S. R.; Novoa, F.; Voroshazi, E.; Dauskardt, R. H. Decohesion Kinetics of PEDOT:PSS Conducting Polymer Films. *Adv. Funct. Mater.* **2014**, *24*, 1325−1332.
(90) Kim, J. H.; Lee, I.; Kim, T. S.; Rolston, N.; Watson, B. L.; Dauskardt, R. H. Understanding Mechanical Behavior and Reliability of Organic Electronic Materials. *MRS Bull.* **2017**, *42*, 115−123.
(91) Tummala, N. R.; Bruner, C.; Risko, C.; Bredas, J. L.; Dauskardt, R. H. Molecular-Scale Understanding of Cohesion and Fracture in P3HT:Fullerene Blends. *ACS Appl. Mater. Interfaces* **2015**, *7*, 9957−9964.
(92) Bruner, C.; Miller, N. C.; McGehee, M. D.; Dauskardt, R. H. Molecular Intercalation and Cohesion of Organic Bulk Heterojunction Photovoltaic Devices. *Adv. Funct. Mater.* **2013**, *23*, 2863−2871.
(93) Corazza, M.; Rolston, N.; Dauskardt, R. H.; Beliatis, M.; Krebs, F. C.; Gevorgyan, S. A. Role of Stress Factors on the Adhesion of Interfaces in R2R Fabricated Organic Photovoltaics. *Adv. Energy Mater.* **2016**, *6*, No. 1501927.
(94) Dupont, S. R.; Voroshazi, E.; Heremans, P.; Dauskardt, R. H. The Effect of Anneal, Solar Irradiation and Humidity on the Adhesion/Cohesion Properties of P3HT:PCBM Based Inverted Polymer Solar Cells. In *2012 38th IEEE Photovoltaic Specialists Conference*; IEEE, 2012; pp. 3259−3262.
(95) Dupont, S. R.; Voroshazi, E.; Nordlund, D.; Dauskardt, R. H. Morphology and Interdiffusion Control to Improve Adhesion and Cohesion Properties in Inverted Polymer Solar Cells. *Sol. Energy Mater. Sol. Cells* **2015**, *132*, 443−449.
(96) Dupont, S. R.; Voroshazi, E.; Nordlund, D.; Vandewal, K.; Dauskardt, R. H. Controlling Interdiffusion, Interfacial Composition, and Adhesion in Polymer Solar Cells. *Adv. Mater. Interfaces* **2014**, *1*, No. 1400135.
(97) Heffner, G. W.; Pearson, D. S. Molecular Characterization of Poly(3-Hexylthiophene). *Macromolecules* **1991**, *24*, 6295−6299.
(98) Tummala, N. R.; Risko, C.; Bruner, C.; Dauskardt, R. H.; Brédas, J. L. Entanglements in P3HT and Their Influence on Thin-Film Mechanical Properties: Insights from Molecular Dynamics Simulations. *J. Polym. Sci. B Polym. Phys.* **2015**, *53*, 934−942.
(99) Mahouche-Chergui, S.; Boussaboun, Z.; Oun, A.; Kazembeyki, M.; Hoover, C. G.; Carbonnier, B.; Ouellet-Plamondon, C. M. Sustainable Preparation of Graphene-like Hybrid Nanomaterials and Their Application for Organic Dyes Removal. *Chem. Eng. Sci.* **2021**, *236*, No. 116482.
(100) Vanlandingham, M. R.; Chang, N. K.; Drzal, P. L.; White, C. C.; Chang, S. H. Viscoelastic characterization of polymers using instrumented indentation. I. Quasi-static testing. *J. Polym. Sci. B Polym. Phys.* **2005**, *43*, 1794−1811.
(101) White, C. C.; Vanlandingham, M. R.; Drzal, P. L.; Chang, N. K.; Chang, S. H. Viscoelastic characterization of polymers using instrumented indentation. II. Dynamic testing. *J. Polym. Sci. B Polym. Phys.* **2005**, *43*, 1812−1824.

https://doi.org/10.1021/acs.chemmater.3c00485
Chem. Mater. 2023, 35, 3329−3342

(102) Li, H.; Randall, N. X.; Vlassak, J. J. New Methods of Analyzing Indentation Experiments on Very Thin Films. *J. Mater. Res.* **2010**, *25*, 728−734.
(103) Oliver, W. C.; Pharr, G. M. An Improved Technique for Determining Hardness and Elastic Modulus Using Load and Displacement Sensing Indentation Experiments. *J. Mater. Res.* **1992**, *7*, 1564−1583.
(104) Fedors, R. F. A method for Estimating Both the Solubility Parameters and Molar Volumes of Liquids. *Polym. Eng. Sci.* **1973**, *14*, 147−154.
(105) Tahk, D.; Lee, H. H.; Khang, D.-Y. Elastic Moduli of Organic Electronic Materials by the Buckling Method. *Macromolecules* **2009**, *42*, 7079−7083.
(106) Savagatrup, S.; Makaram, A. S.; Burke, D. J.; Lipomi, D. J. Mechanical Properties of Conjugated Polymers and Polymer-Fullerene Composites as a Function of Molecular Structure. *Adv. Funct. Mater.* **2014**, *24*, 1169−1181.
(107) Choudhary, K.; Chen, A. X.; Pitch, G. M.; Runser, R.; Urbina, A.; Dunn, T. J.; Kodur, M.; Kleinschmidt, A. T.; Wang, B. G.; Bunch, J. A.; Fenning, D. P.; Ayzner, A. L.; Lipomi, D. J. Comparison of the Mechanical Properties of a Conjugated Polymer Deposited Using Spin Coating, Interfacial Spreading, Solution Shearing, and Spray Coating. *ACS Appl. Mater. Interfaces* **2021**, *13*, 51436−51446.
(108) Xie, R.; Weisen, A. R.; Lee, Y.; Aplan, M. A.; Fenton, A. M.; Masucci, A. E.; Kempe, F.; Sommer, M.; Pester, C. W.; Colby, R. H.; Gomez, E. D. Glass Transition Temperature from the Chemical Structure of Conjugated Polymers. *Nat. Commun.* **2020**, *11*, 893.
(109) Chen, S.-A.; Ni, J.-M. Structure/Properties of Conjugated Conductive Polymers. 1. Neutral Poly(3-Alkylthiophene)S. *Macromolecules* **1992**, *25*, 6081−6089.
(110) Khlyabich, P. P.; Rudenko, A. E.; Burkhart, B.; Thompson, B. C. Contrasting Performance of Donor-Acceptor Copolymer Pairs in Ternary Blend Solar Cells and Two-Acceptor Copolymers in Binary Blend Solar Cells. *ACS Appl. Mater. Interfaces* **2015**, *7*, 2322−2330.
(111) Koch, F. P. V.; Smith, P.; Heeney, M. "Fibonacci's Route" To Regioregular Oligo(3-Hexylthiophene)S. *J. Am. Chem. Soc.* **2013**, *135*, 13695−13698.
(112) Zhao, B.; Awartani, O.; O'Connor, B.; Zikry, M. A. A Direct Correlation of X-Ray Diffraction Orientation Distributions to the in-Plane Stiffness of Semi-Crystalline Organic Semiconducting Films. *Appl. Phys. Lett.* **2016**, *108*, 181902.
(113) Qiao, X.; Wang, X.; Mo, Z. Effects of Different Alkyl Substitution on the Structures and Properties of Poly(3-Alkylthiophenes). *Synth. Met.* **2001**, *118*, 89−95.
(114) Park, H.; Han, M. J.; Kim, Y.; Kim, E. J.; Kim, H. J.; Yoon, D. K.; Kim, B. J. Regioregularity-Dependent Crystalline Structures and Thermal Transitions in Poly(3-Dodecylthiophene)S. *Chem. Mater.* **2021**, *33*, 3312−3320.
(115) Mcbride, M.; Zhang, G.; Grover, M.; Reichmanis, E. Poly(3-Alkylthiophenes): Controlled Manipulation of Microstructure and Its Impact on Charge Transport. In *Conjugated Polymers: Properties, Processing, and Applications*; CRC Press, 2019; pp. 351−389.
(116) Qian, Z.; Luo, S.; Qu, T.; Galuska, L. A.; Zhang, S.; Cao, Z.; Dhakal, S.; He, Y.; Hong, K.; Zhou, D.; Gu, X. Influence of Side-chain Isomerization on the Isothermal Crystallization Kinetics of Poly(3-alkylthiophenes). *J. Mater. Res.* **2021**, *36*, 191−202.
(117) Jiang, K.; Wang, L.; Zhang, X.; Song, Y.; Zhang, W. Side-Chain Length Dependence of Young's Modulus and Strength in Crystalline Poly(3-Alkylthiophene) Nanofibers. *Macromolecules* **2020**, *53*, 10061−10068.
(118) Xu, W.; Li, L.; Tang, H.; Li, H.; Zhao, X.; Yang, X. Solvent-Induced Crystallization of Poly(3-Dodecylthiophene): Morphology and Kinetics. *J. Phys. Chem. B* **2011**, *115*, 6412−6420.
(119) Maksimov, R. D.; Plume, E. Z.; Jansons, J. O. Comparative Studies on the Mechanical Properties of a Thermoset Polymer in Tension and Compression. *Mech. Compos. Mater.* **2005**, *41*, 425−436.
(120) Chen, W.; Lu, F.; Cheng, M. Tension and Compression Tests of Two Polymers under Quasi-Static and Dynamic Loading. *Polym. Test.* **2002**, *21*, 113−121.
(121) Deblieck, R. A. C.; Van Beek, D. J. M.; Remerie, K.; Ward, I. M. Failure Mechanisms in Polyolefines: The Role of Crazing, Shear Yielding and the Entanglement Network. *Polymer* **2011**, *52*, 2979−2990.
(122) Donald, A. M.; Kramer, E. J. The Competition between Shear Deformation and Crazing in Glassy Polymers. *J. Mater. Sci.* **1982**, *17*, 1871−1879.
(123) Kramer, E. J.; Berger, L. L. Fundamental Processes of Craze Growth and Fracture. In *Crazing in Polymers*; *Advances in Polymer Science*; Springer: 1990; Vol. *2*, p. 68.
(124) Cao, Z.; Galuska, L.; Qian, Z.; Zhang, S.; Huang, L.; Prine, N.; Li, T.; He, Y.; Hong, K.; Gu, X. The Effect of Side-Chain Branch Position on the Thermal Properties of Poly(3-Alkylthiophenes). *Polym. Chem.* **2020**, *11*, 517−526.
(125) Gent, A. N.; Petrich, R. P. Adhesion of Viscoelastic Materials To Rigid Substrates. *Proc. R. Soc. A.* **1969**, *310*, 433−448.
(126) Krenceski, M. A.; Johnson, J. F.; Temin, S. C. Chemical and Physical Factors Affecting Performance of Pressure-Sensitive Adhesives. *J. Macromol. Sci. C* **1986**, *26*, 143−182.
(127) Payra, D.; Fujii, Y.; Das, S.; Takaishi, J.; Naito, M. Rational Design of a Biomimetic Glue with Tunable Strength and Ductility. *Polym. Chem.* **2017**, *8*, 1654−1663.
(128) Hutchinson, J. W.; Evans, A. G. Mechanics of Materials: Top-down Approaches to Fracture. *Acta Mater.* **2000**, *48*, 125−135.
(129) Schmitt, A.; Samal, S.; Thompson, B. C. Tuning the Surface Energies in a Family of Poly-3-Alkylthiophenes Bearing Hydrophilic Side-Chains Synthesized: Via Direct Arylation Polymerization (DArP). *Polym. Chem.* **2021**, *12*, 2840−2847.
(130) Howard, J. B.; Ekiz, S.; Noh, S.; Thompson, B. C. Surface Energy Modification of Semi-Random P3HTT-DPP. *ACS Macro Lett.* **2016**, *5*, 977−981.
(131) Howard, J. B.; Noh, S.; Beier, A. E.; Thompson, B. C. Fine Tuning Surface Energy of Poly(3-Hexylthiophene) by Heteroatom Modification of the Alkyl Side Chains. *ACS Macro Lett.* **2015**, *4*, 725−730.
(132) Maugis, D. Subcritical Crack Growth, Surface Energy, Fracture Toughness, Stick-Slip and Embrittlement. *J. Mater. Sci.* **1985**, *20*, 3041−3073.
(133) Robinson, L.; Isaksson, J.; Robinson, N. D.; Berggren, M. Electrochemical Control of Surface Wettability of Poly(3-Alkylthiophenes). *Surf. Sci.* **2006**, *600*, L148.
(134) Kanai, K.; Miyazaki, T.; Suzuki, H.; Inaba, M.; Ouchi, Y.; Seki, K. Effect of Annealing on the Electronic Structure of Poly(3-Hexylthiophene) Thin Film. *Phys. Chem. Chem. Phys.* **2010**, *12*, 273−282.
(135) Son, S. Y.; Park, T.; You, W. Understanding of Face-On Crystallites Transitioning to Edge-On Crystallites in Thiophene-Based Conjugated Polymers. *Chem. Mater.* **2021**, *33*, 4541−4550.
(136) Blau, R.; Chen, A. X.; Polat, B.; Becerra, L. L.; Runser, R.; Zamanimeymian, B.; Choudhary, K.; Lipomi, D. J. Intrinsically Stretchable Block Copolymer Based on PEDOT:PSS for Improved Performance in Bioelectronic Applications. *ACS Appl. Mater. Interfaces* **2022**, *14*, 4823−4835.
(137) Persson, B. N. J.; Tosatti, E. The Effect of Surface Roughness on the Adhesion of Elastic Solids. *J. Chem. Phys.* **2001**, *115*, 5597−5610.
(138) Gent, A. N.; Lin, C. W. Model Studies of the Effect of Surface Roughness and Mechanical Interlocking on Adhesion. *J. Adhes.* **1990**, *32*, 113−125.
(139) Katainen, J.; Paajanen, M.; Ahtola, E.; Pore, V.; Lahtinen, J. Adhesion as an Interplay between Particle Size and Surface Roughness. *J. Colloid Interface Sci.* **2006**, *304*, 524−529.
(140) Kim, W. S.; Yun, I. H.; Lee, J. J.; Jung, H. T. Evaluation of Mechanical Interlock Effect on Adhesion Strength of Polymermetal Interfaces Using Micro-Patterned Surface Topography. *Int. J. Adhes. Adhes.* **2010**, *30*, 408−417.
(141) Libanori, R.; Carnelli, D.; Rothfuchs, N.; Binelli, M. R.; Zanini, M.; Nicoleau, L.; Feichtenschlager, B.; Albrecht, G.; Studart, A. R. Composites Reinforced via Mechanical Interlocking of Surface-

https://doi.org/10.1021/acs.chemmater.3c00485
Chem. Mater. 2023, 35, 3329−3342

Roughened Microplatelets within Ductile and Brittle Matrices. *Bioinspir. Biomim.* **2016**, *11*, No. 036004.
(142) Fuller, K. N. G.; Tabor, D. The Effect of Surface Roughness on the Adhesion of Elastic Solids. *Proc. R. Soc. Lond. A.* **1975**, *345*, 327−342.

https://doi.org/10.1021/acs.chemmater.3c00485
Chem. Mater. 2023, 35, 3329−3342